We are IntechOpen, the world's leading publisher of Open Access books Built by scientists, for scientists

4,800
Open access books available

122,000
International authors and editors

135M
Downloads

Our authors are among the

154
Countries delivered to

TOP 1%
most cited scientists

12.2%
Contributors from top 500 universities

CLARIVATE ANALYTICS BOOK CITATION INDEX INDEXED

WEB OF SCIENCE™

Selection of our books indexed in the Book Citation Index in Web of Science™ Core Collection (BKCI)

Interested in publishing with us?
Contact book.department@intechopen.com

Numbers displayed above are based on latest data collected.
For more information visit www.intechopen.com

Chapter 10

Thermoelectric Power Generation by Clathrates

Andrei V. Shevelkov

Additional information is available at the end of the chapter

http://dx.doi.org/10.5772/65600

Abstract

Clathrate compounds combine aesthetic beauty of their crystal structures with promising thermoelectric properties that have made them one of the most explored family of compounds deemed as base for thermoelectric generators for mid- and high-temperature application. This chapter surveys crystal and electronic structure and structure-related transport properties of selected types of clathrates and discusses their thermoelectric performance and prospects of their future applications.

Keywords: thermoelectric materials, thermoelectric power generation, clathrates, phonon glass-electronic crystal, charge carrier transport, heat transport

1. Introduction

No compound is able to outplay properly doped bismuth telluride as material for thermoelectric cooling. Since the pioneer works of A.F. Ioffe in the 1950, this material solely holds the position in the industry [1]. Situation is different, when it comes to thermoelectric power generation, where traditional materials based on Bi_2Te_3 are giving way to new state-of-the-art materials. Among the latter, there are clathrates; these compounds combine low, glass-like thermal conductivity with high electrical conductivity and Seebeck coefficient and are demanded as perspective thermoelectric materials that convert temperature gradient into electric power [2–4].

Clathrates are different from many other prospective materials for thermoelectric power generators, because they feature the spatial separation of two substructures known as host clathrate framework and rattling guests [4–6]. The framework is based on strong covalent bonds, four for each atom, that ensure effective transport of charge carriers leading to high values of both electrical conductivity and thermopower, whereas the rattling of guests inside oversized cages of the framework causes low thermal conductivity owing to either scattering

of heat-carrying phonons or reducing phonon group velocity due to avoided crossing of rattling modes and branches of acoustic phonons. The spatial host-guest separation provides the base for practical utilization of "phonon glass-electron crystal" (PGEC) concept introduced by Slack, according to which decoupling of heat and charge carriers transport enables their independent optimization [7]. But despite the spatial separation, thermal and charge carriers transport properties are not truly independent, which makes optimization of thermoelectric efficiency a very intricate and delicate task. Recent years have witnessed appreciable progress in enhancing thermoelectric efficiency of clathrates at mid- and high-temperature regions. The phonon engineering approaches, including introduction of rare earth guests and formation of complex superstructures, have led to extremely low thermal conductivity for narrow-gap clathrate semiconductors. New synthetic approaches have enabled accurate tuning of charge carriers' concentration by extremely precise doping, as well as providing very high densities of properly consolidated ceramic materials. Finally, new compositions of clathrates have emerged, that allow combination of reasonably high thermoelectric efficiency and utmost chemical and thermal stability. Already now, there are examples of clathrate compounds displaying high values of figure-of-merit, even surpassing unity at T > 470 K, and further progress is highly expected.

This chapter surveys recent progress in developing thermoelectric materials for power generation on the base of inorganic clathrate compounds. We consider crystal and electronic structures of these compounds, the underlying physics of their thermoelectric properties, synthetic methods of their preparation, and, as a central issue, their thermoelectric performance. Current achievements and future prospects are discussed.

2. Clathrates as inclusion compounds

2.1. Crystal structures

Clathrates belong to plentiful class of inclusion compounds. Their discovery is traced back to the beginning of the nineteenth century, when Sir Davy observed formation of solid chlorine hydrate upon passing gaseous chlorine through water cooled to +5°C. Other hydrates came soon after, and by the middle of the twentieth century, quite a number of hydrates of various gases and liquids were discovered, and their crystal structures were solved. Despite clear differences in their chemical composition and crystal structures, these compounds shared a single common feature, which is complete sequestering of a guest moiety inside cages of framework. Another distinct feature of those compounds is the absence of strong host-guest bonds. In 1965 [8], Kasper, Hagenmuller, and Pouchard reported two new sodium silicides, whose crystal structures were identical to hydrates of various gases, proving that host-guest size matching had the primary role in their formation and stability, rather than the details of chemical bonding. Since then, almost three hundred compounds belonging to ten structure types were documented [3–5, 9]. They involve almost 50 chemical elements constituting more than 50% of all stable chemical elements (**Figure 1**).

http://dx.doi.org/10.5772/65600

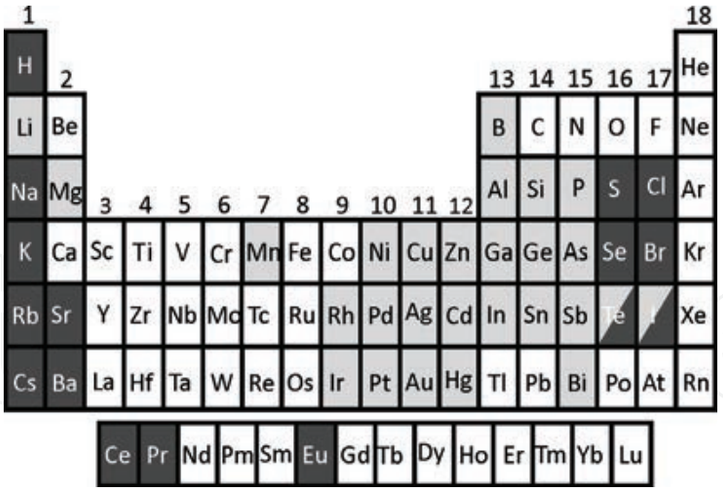

Figure 1. "Clathrate Periodic Table."

All clathrate crystal structures are based on closed polyhedra having from 20 to 28 vertices (**Figure 2**). Various combinations of these polyhedra lead to complete filling of the space, which is distinctive feature of clathrates. In this review, we will focus on four clathrates types, known as type-I, type-II, type-III, and type-VIII clathrates, as many of them demonstrate high thermoelectric figure-of-merit, in part stemming from the details of their crystal structure.

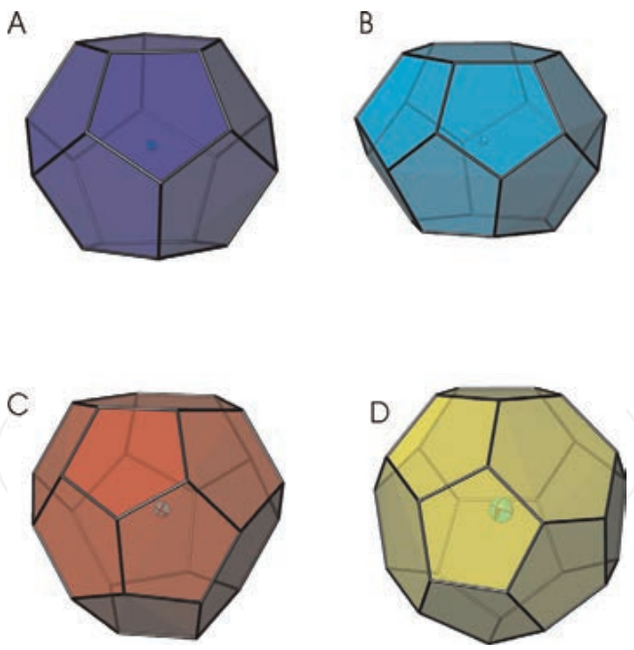

Figure 2. Clathrate-forming polyhedra: (a) 20-vertex pentagonal dodecahedron; (b) 24-vertex tetrakaidecahedron; (c) 26-vertex pentakaidecahedron; and (d) 28-vertex hexakaidecahedron.

Clathrates of type-I are the most numerous; recent review lists over 100 representatives of this structure type [10]. Their crystal structure consists of two types of polyhedra, 20-vertex dodecahedron and 24-vertex tetrakaidecahedron. The latter polyhedra form three-dimension-

al cubic array in such a way, that centers of adjacent 6-member rings form close rod packing, as in the crystal structure of Cr_3Si, whereas the smaller polyhedra fill the remaining empty space (**Figure 3**). Guest atoms fill the centers of the polyhedra, forming only long, non-covalent contacts with atoms forming polyhedral framework. The resulting crystal structure belongs to cubic space group Pm3n and has general chemical formula $E_{46}G_8$, which emphasizes that there are 46 framework atoms and eight guest atoms per unit cell. Whereas the guest atoms occupy two positions, sixfold inside the larger polyhedral cage and twofold inside the smaller one, and have very large coordination numbers of 24 and 20, respectively, all atoms of the framework (24-fold, 16-fold, and sixfold) have tetrahedron environment.

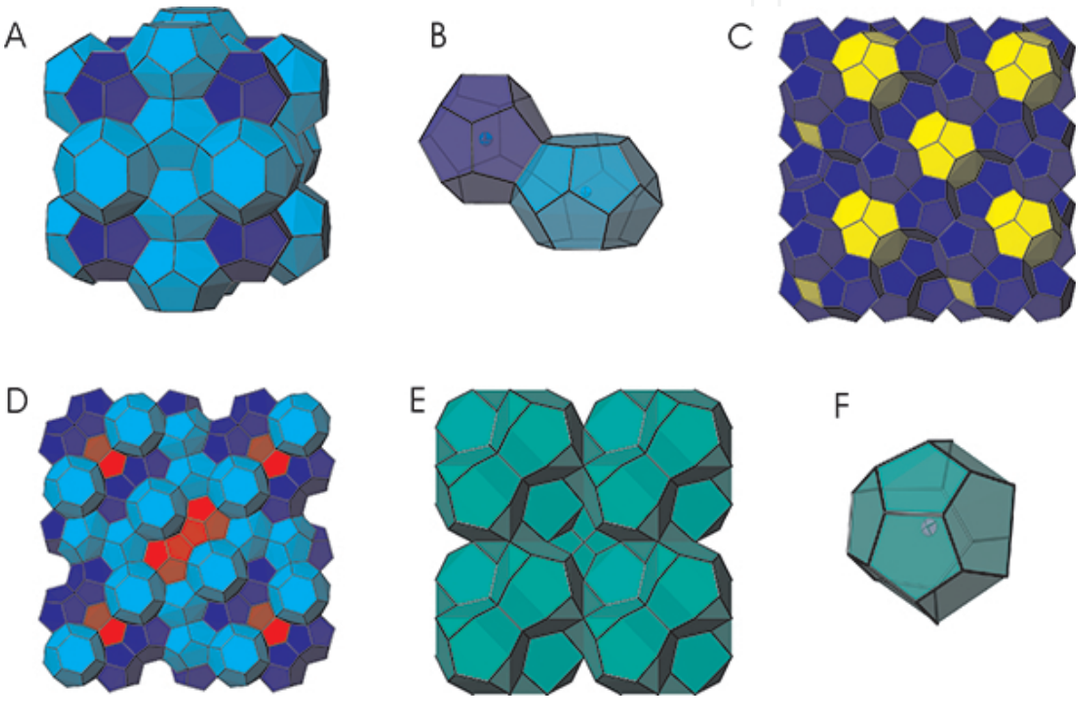

Figure 3. Crystal structure of clathrates: (A) type-I clathrate; (B) two adjacent polyhedra in type-I clathrate; (C) type-II clathrate; (D) type-III clathrate; (E) type-VIII clathrate; and (F) asymmetric cage in type-VIII clathrate.

The nature of chemical elements that form type-I clathrates is quite diverse. In general, type-I clathrates are classified into two groups depending on charge of the framework. The most numerous are anionic clathrates, in which the framework bears negative charge compensated by guest cations. A reverse of the host-guest polarity leads to cationic (also known as inversed) clathrates. As a rule, atoms that form framework come from *p*-block of Mendeleev periodic table; however, inclusion of *d*-metals is also possible. Guest atoms are different depending on charge of the framework. In anionic clathrates, guests are cations of large alkali or alkali earth metals; only a few examples of clathrates hosting rare earth metals are documented [11–13]. In the case of cationic clathrates, halogens and chalcogens of 3–5 periods of Mendeleev table serve as anionic guests.

Type-I clathrates frequently feature deviations from ideal crystal structure described above. This includes mixed occupancy of positions by atoms of different chemical nature, partially

vacant positions, splitting of positions into two or three closely lying partial occupied sites, and various types of atom and vacancy ordering that lead to formation of superstructures and reduction in symmetry [10]. In most cases, these crystallographic details affect the electronic structure of clathrates and invoke properties that enhance thermoelectric efficiency.

Other clathrate types are less numerous. Their crystal structures are also built of different high-coordination polyhedra. For instance, type-II clathrate is made of combination of 20-vertex dodecahedra with 28-vertex hexakaidecahedra in such a fashion that cubic face-centered structure is formed (**Figure 3**). Crystal structure of type-III clathrates is the only clathrate structure that contains three types of polyhedra at the time; they are 20-vertex dodecahedra, 24-vertex tetrakaidecahedra, and 26-vertex pentakaidecahedra. They share faces to form a tetragonal crystal structure displayed in **Figure 3**. Type-VIII clathrates are slightly different as they have only one type of polyhedra, which is substantially distorted. It can be viewed as dodecahedron, in which three E–E bonds are broken, and three extra E atoms are inserted instead. The resulting polyhedron has rather low symmetry, but its packing within cubic unit cell brings about clathrate type of the crystal structure. As long as distorted polyhedra cannot fill the entire space, additional 8-vertex polyhedra are left unfilled in this crystal structure (**Figure 3**).

2.2. Application of Zintl scheme and electronic structures

Chemical composition of clathrates frequently looks unusual in terms of the stoichiometry of phases. For instance, the following compounds displaying promising thermoelectric properties are formulated as $Sr_8Ga_{16}Ge_{30}$, $Ba_8Ga_{16}Sn_{30}$, $K_8In_8Sn_{38}$, and $Si_{30}P_{16}Te_8$. These formulas can be rationalized on the basis of Zintl electron-counting scheme, which, in fact, shows that these compounds should behave as semiconductors [14].

Application of Zintl scheme rests on the tetrahedral coordination of all atoms of the framework. They all form four two-center, two-electron (2c–2e) bonds, thus forming electronic octet. Let us consider clathrate compound with formula $Ba_8Ga_{16}Sn_{38}$. Its framework comprises tetrahedrally bonded Ga and Sn atoms, whereas Ba guests compensate for the charge of the framework. Each Sn atom forms four 2c–2e bonds, for which it uses four own electrons and four electrons shared with four neighbors. Therefore, it does not require loss or gain of further electrons, which means that under Zintl scheme its formal oxidation state is zero. Similarly, Ga atom, having three valence electrons, is one electron short of forming four 2c–2e bonds. It must gain one electron to achieve an octet, thus acquiring formal oxidation state of −1. There are 16 Ga atoms per formula, which requires compensating for 16 negative charges. Ba atoms with coordination numbers of 20 and 24 clearly exist as Ba^{2+} cations. There are eight +2 cations that compensate for the charge of the framework and ensure the overall electroneutrality of $Ba_8Ga_{16}Sn_{30}$.

The overall electroneutrality of clathrate compound along with formation of electron octets makes these compounds semiconductors unless limitations of Zintl scheme are overcome. This may happen under various circumstances, including an introduction of *d*-metal into framework, combination of elements, that would lead to overlap of valence and conduction bands, and energy gain of accepting or expelling an electron in favor of formation of chemical bond

of high bond energy, as in the case of Si–Si bond [15]. In such cases, metal-to-insulator transition (MIT) may occur, leading to temperature-dependent properties, with prospective thermoelectric parameters at the verge of MIT.

Electronic structure of clathrates, albeit having little in common with Zintl counting scheme, still shows the propensity of this compounds to behave as semiconductors [14]. Electronic structure of various clathrates has been assessed in numerous reports and discussed in several reviews [3–6]. However, the majority of the studies are dealing with calculations at different levels. For type-I clathrates, it was shown that fulfillment of Zintl rule shows up in the following way: All bonding states and, if necessary, nonbonding states (lone pairs neighboring vacancies) are filled and lie below Fermi level, whereas all antibonding states are empty and compose conduction band. Common feature of band structure is that the states in vicinity of Fermi level are composed predominantly by individual contributions that are the most sensitive to various substitutions within clathrate framework. For instance, in type-I clathrate, $Sn_{24-x}In_xP_{22}I_8$ indium orbitals have the largest contribution to the states just below Fermi level [16]. In $Sn_{24}P_{19.3}I_8$, another type-I clathrate, but with vacancies in the positions of phosphorus, lone pairs on tin atoms, that surround vacancies, cluster together to form sharp states at the top of valence band [17] (**Figure 4**). Therefore, minor changes in concentration of vacancies or doping element can substantially alter transport properties of clathrates.

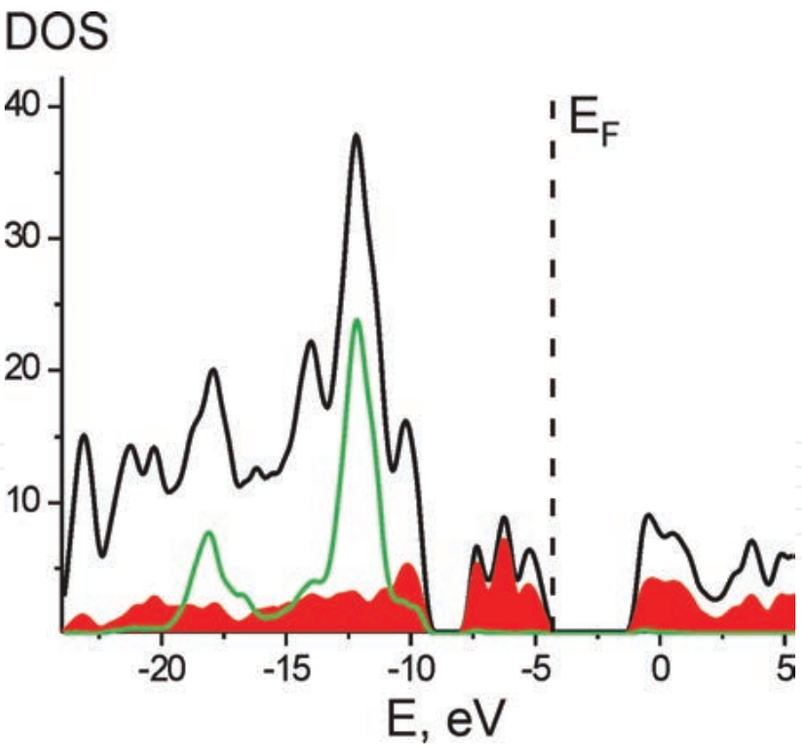

Figure 4. Scheme of the band structure of $Sn_{24}P_{19.3}I_8$ presented as density of states (DOS) versus energy. Black, total DOS; green, contribution of 4-bonded Sn; red, contribution of 3 + 3-bonded Sn.

Experimental studies of the electronic structure of clathrates are very rare. This is explained by necessity to have rather large single crystals and clean surface to investigate electronic

http://dx.doi.org/10.5772/65600

structure by means of X-ray photoelectron spectroscopy (XPS). Recently, these obstacles were overcome, and comprehensive picture of electronic band structure of type-I clathrate $Sn_{24-x}In_xAs_{22}I_8$ was obtained [18]. This study proves that chemical bonding has different nature; within the framework, strong covalent bonds are present, whereas the host-guest interactions have pronounced electrostatic nature with clear transfer of electrons from the framework atoms toward guest iodine species. Further, it is shown that top of valence band is composed of shallow I 5*p*, As 4*p*, In 5*p*, and Sn 5*p* orbitals that are largely mixed (**Figure 5**).

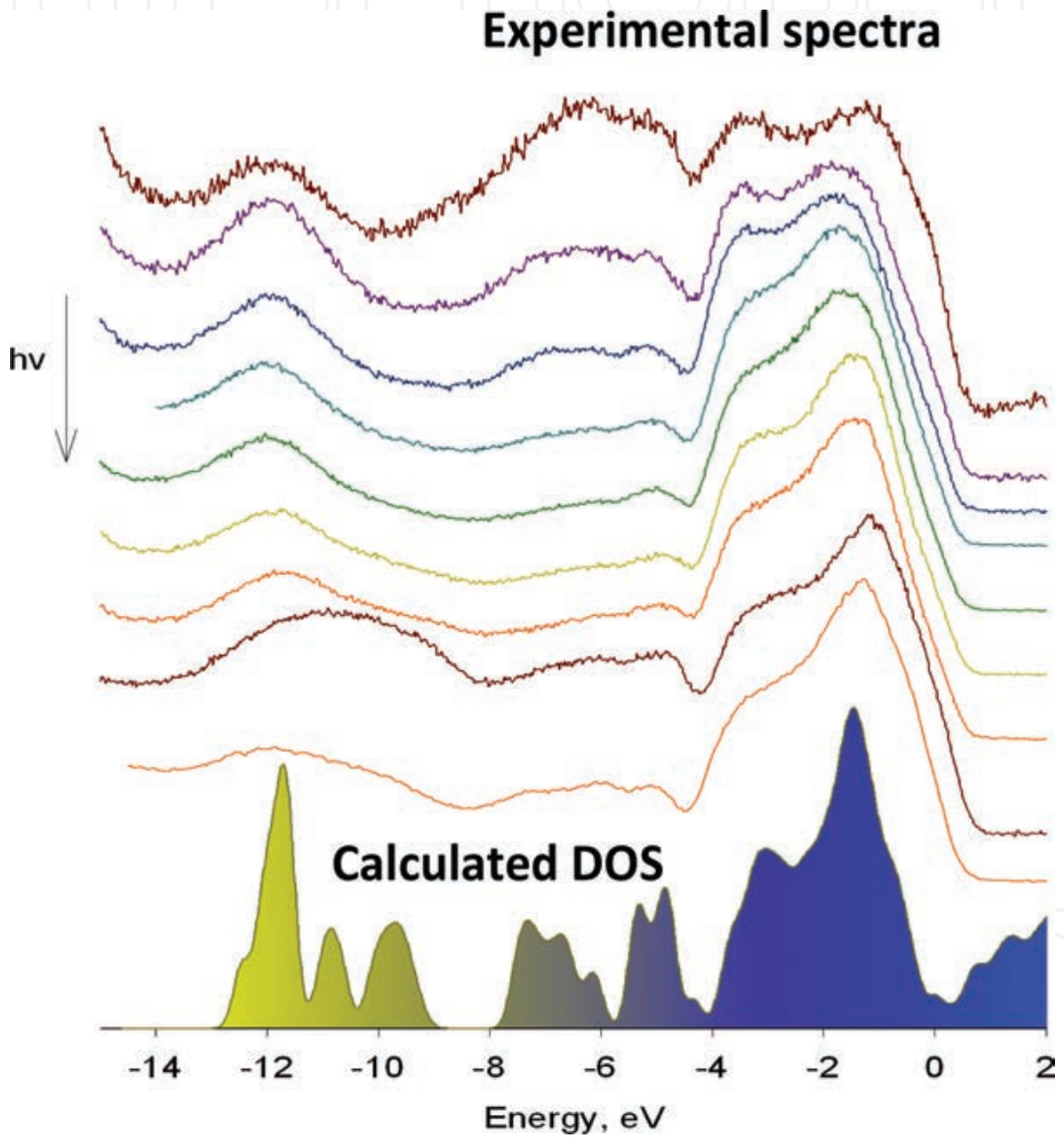

Figure 5. Experimental and calculated electronic band structure of $Sn_{22-x-\delta}In_xAs_{22-y}I_8$ for $x = 12$. Reprinted with permission from Inorg. Chem. 2015, 54, 11542–11549. Copyright 2015 American Chemical Society.

In contrast to majority of clathrate types, where semiconducting properties are hardly violated, in the case of type-II clathrates, metallic behavior is more norm than exception. Most of type-II clathrates feature frameworks made of single kind of atoms, $Na_{24-x}Si_{136}$ being a typical example [19]. In these clathrates, the strength of Si-Si bond (226 kJ/mol) outplays energy loss

associated with filling the bottom of conduction band by electrons upon occupation of the guest sites by sodium. Depending on concentration of the guest atoms, MIT is expected, which may lead to various interesting properties, including high thermoelectric performance [20].

3. Sample preparation

3.1. Synthesis and crystal growth

Synthetic routes to clathrates are different. They largely depend on the nature of elements constituting a particular compound. High-temperature ampoule synthesis is the most common method for preparing clathrate compounds, the exact temperature depending on the chemical system. The highest temperatures are explored in the case of silicon-based clathrates owing to very low reactivity of silicon. Heating up to 1500 K might be necessary to enroll this element into reaction; for instance, type-III clathrate $Si_{130}P_{42}Te_{21}$ was synthesized by heating the stoichiometric mixture of elemental components at 1425 K for 18 days [21]. Further prolonged annealing with intermediate regrinding is always required to achieve homogeneous product. Lower temperatures, between 800 and 1250 K, are required by less inert germanium. For comparison with the previous example, we note that to synthesize isostructural type-III clathrate $Ge_{130}P_{42}Te_{21}$, temperature of 953 K was sufficient. Completely different scenario is realized in the case of tin. The latter element has low melting point of 505 K, and preparation of tin-based clathrates is associated with formation of melts rich in tin. This frequently becomes an obstacle, because surface of melted tin becomes covered with poorly reactive compounds, such as Sn_4P_3 or SnAs, leading to incomplete reaction of precursors [18]. This obstacle can be overcome by introducing vapor transport agents. For instance, elemental iodine or SnI_4 tend to facilitate reactions owing to formation of volatile intermediates [22, 23].

Other synthetic methods include flux synthesis, precursor decomposition, high-pressure synthesis, and oxidation in ionic liquids [14]. They are used in selected cases depending on the properties of desired clathrates. Of those methods, flux synthesis is rather intensively used both for synthesis and for crystal growth when such low-melting metals as gallium or tin or even aluminum are included in chemical composition of clathrates. Metals themselves produce flux and at the same time are used as reactants. In some cases, large crystals with mass up to 60 mg were prepared by pulling from the melt [24]. A peculiar variation of this method was used for growing crystals of thermoelectric clathrate $Ba_8Ga_{16}Sn_{30}$, where two *p*-metals, gallium and tin, were used as common flux, and properties of the resulting crystals strongly depended on which metal was taken in excess [25].

3.2. Sample densification

As clathrates are deemed as prospective thermoelectric materials, the problem of sample densification is put forward. Only for a limited number of clathrates, cold pressing produces samples with the density up to 85% of theoretical. These cases are limited to tin-based compounds that exhibit less rigid clathrate frameworks [26].

http://dx.doi.org/10.5772/65600

In recent years, major success in preparing dense samples of various clathrates has been achieved by using of spark plasma sintering (SPS). This method is based on a simultaneous application of temperature, pressure, and DC pulses to sample under inert atmosphere or vacuum (**Figure 6**). High-energy DC pulses are believed to excite plasma nearest to intergrain contacts, leading to high local overheating and consequent bridging of grains with formation of larger uniform particles. Although the exact mechanism is not known and the very formation of plasma is sometimes questioned, this method has been successfully used for preparation of many types of materials [27]. In particular, SPS allows synthesis of clathrates at lower temperatures and lower pressures compared to standard high-pressure method, which is very advantageous as long as clathrates cannot withstand too high pressure because of readily collapse of their tracery framework [28]. For instance, compact and dense pellets of $Ge_{30}P_{16}Se_8$ could be prepared at temperature of 773 K and pressure of 60 MPa that already provided sample density of 96% relative to theoretical one [29]. Similarly, silicon-based clathrates were densified at significantly harsher condition of 1100 K and 110 MPa to achieve sample density of 95% [21, 30]. In both cases, no degradation of the initial sample was observed, proving that densification does not change composition and structure of clathrates and that concomitant thermoelectric measurements are performed on the samples of desired nature.

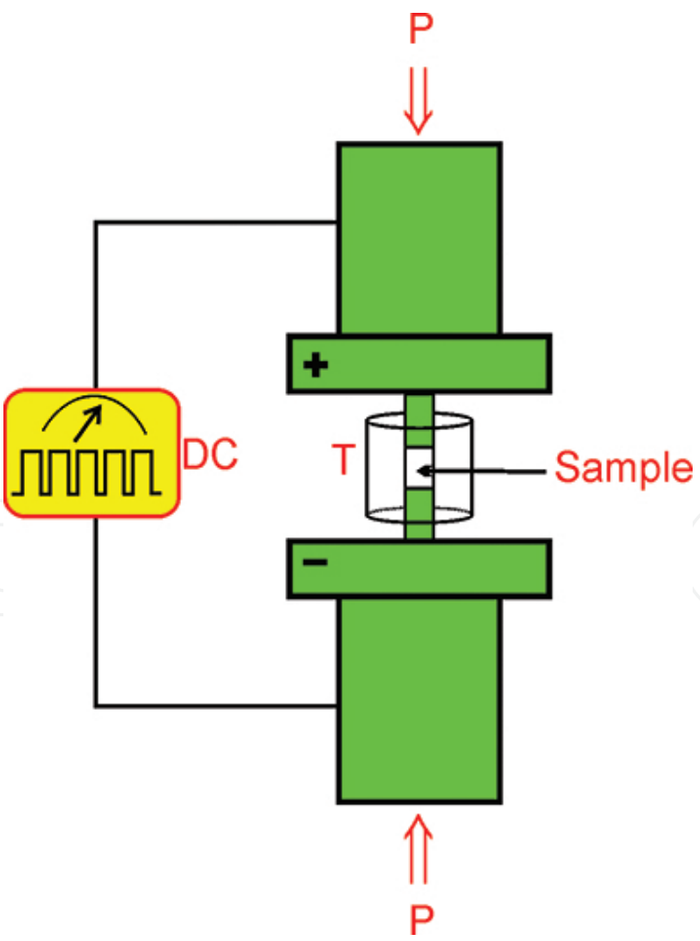

Figure 6. Scheme of the SPS method.

4. Transport properties

4.1. Charge carriers transport

As long as clathrates belong to the family of Zintl compounds, they frequently display activation type of conductivity typical for proper semiconductors. They possess rather high values of electrical conductivity, σ, and Seebeck coefficient, S, giving rise to moderately high values of power factor, $S^2\sigma$. The latter describes transport of charge carries and depends largely on details of the band structure of given compounds.

The advantageous property of clathrates is that their crystal structure, in particular, the spatial separation of host and guest substructures, provides opportunities for tuning charge carriers transport almost independently of phonon transport.

Electrical conductivity of type-I clathrates ranges from several S m^{-1} for ideally balanced compounds to nearly 10^5 S m^{-1} for properly doped semiconductors. For instance, $Sn_{20.5}As_{22}I_8$ has room-temperature electrical conductivity just below 1 S m^{-1}, whereas introduction of In as doping element pushes electrical conductivity to 135–461 S m^{-1} depending on concentration of indium and corresponding vacancies in clathrate framework [16, 31]. Similarly, stoichiometric $Si_{30}P_{16}Te_8$ is not good electrical conductor with room-temperature value of 63.3 S m^{-1} [32]. However, its band structure can be altered upon creating vacancies in guest positions with concomitant change in the Si:P ratio. As a result, band gap was decreased from 1.24 eV to minimum of 0.12 eV and electrical conductivity was increased up to (1–4) × 10^4 S m^{-1} depending on actual composition of clathrate [30]. Importantly, electronic structure and, hence, conducting properties are only weakly sensitive to isovalent substitution, provided that the substituting atoms reside on similar crystallographic sites. For instance, $K_8M_8Sn_{38}$ (M = Al, Ga, and In) exhibits almost the same room-temperature conductivity of (6.5–12.5) × 10^4 S m^{-1} [33]. In these compounds, small change in electrical conductivity can be attributed to shrinkage of clathrate framework upon going from In to Ga and to Al. Another example of sensitivity of transport properties to the framework structural modification is provided by $Sn_{20}Zn_4P_{21.2}X_8$ (X = Br, I). When Br is a guest, the shrinkage of the framework leads to relaxation of atoms residing next to vacancies causing a significant shortage of Sn–P and Zn–P bonds compared to I-based compound. Accordingly, the framework becomes more conductive as band gap decreases from 0.25 to 0.11 eV. As a result, $Sn_{20}Zn_4P_{21.2}Br_8$ displays much greater room-temperature conductivity of 250 S m^{-1} compared to 0.4 S m^{-1} for I-based analog prepared under the same conditions [23].

Basically, electrical conductivity is product of charge, charge carriers' concentration, and mobility. The former is constant, but two other parameters vary with both temperature and chemical nature of clathrate. However, charge carriers' concentration is intrinsic property of a given composition, whereas their mobility is sensitive to grain boundaries. Therefore, observed conductivity of compound with a given composition may depend upon preparation and compacting methods. Type-I clathrate $Sn_{24}P_{19.3}I_8$ provides example of drastic change in electrical conductivity in response to different preparation routes. As-prepared and cold-pressed samples display room-temperature conductivity of 335 S m^{-1}, whereas SPS-treated

sample shows much higher conductivity of 6.5×10^3 S m^{-1} [17, 26]. Temperature-dependent impedance spectroscopy measurements showed that for SPS-compacted sample of high density (92% of theoretical), intergrain contacts start to contribute significantly to total impedance only below 75 K, while above this temperature only activation part could be detected [34].

Importantly, electrical conductivity can be suppressed significantly by significant disorder of crystal structure, which is exemplified by very low value of $\sigma \approx 1$ S m^{-1} at 300 K for $Sn_{20.5}As_{22}I_8$, which is four orders of magnitude smaller than for phosphorus analog. The only reason for such difference is reported to be tremendous disorder in crystal structure of As-based compound, leading to significant scattering of charge carriers on flaws of crystal structure [31].

At high temperatures, many clathrates demonstrate very high electrical conductivity, showing that no other mechanism than activation has any noticeable contribution. There are rare cases of pure metallic properties, where electrical conductivity decreases with temperature as for $Na_{22}Si_{136}$ [19]; considerably more numerous are examples of clathrates lying at the border of metallic and semiconducting regimes and showing slight increase in electrical conductivity with temperature. For instance, type-III clathrate $Si_{132}P_{42}Te_{21}$ displays only threefold increase in electrical conductivity upon heating from 300 to 1100 K [35]. At low temperatures, majority of clathrates display very high electrical resistivity. Noticeably, several Si-based clathrates possess transition into superconducting states below 10 K. For instance, type-I clathrate Ba_8Si_{46} has T_C of 8 K [36], and type-IX clathrate Ba_6Ge_{25} turns on superconducting below 3.8 K [37].

Type-II clathrates are different from those of other types in displaying metallic type of electrical conductivity, and many of them behave as normal metals. In particular, $Cs_8Na_{16}Si_{136}$ and $Cs_8Na_{16}Ge_{136}$ combine high electrical conductivity manifested by smooth increase in electrical resistivity with temperature-independent Pauli paramagnetism; such combination is typical for good metals [38].

Clathrates demonstrate different types of majority carriers, and therefore, Seebeck coefficient can be positive (holes) or negative (electrons). Absolute values of Seebeck coefficients vary from one clathrate to another and depend on multifold factors. They include band gap width, concentration of charge carriers, degree of the framework disorder, and many others. In most cases, as generally observed for proper semiconductors, the higher the electrical conductivity is, the lower the Seebeck coefficient is, which stems from the opposite trend of their dependence upon charge carriers' concentration [1, 3]. This is exemplified by several clathrates of different structure types. Whereas type-I $Sn_{24}P_{19.3}I_8$ demonstrates at 300 K high electrical conductivity of 6.5×10^3 S × m^{-1}, but also exhibits rather low Seebeck coefficient of only +80 μV × K^{-1}, formally isostructural compound $Ge_{38}Sb_8I_8$ displays very high Seebeck coefficient of about +800 μV × K^{-1}, and its electrical conductivity does not exceed 10^{-1} S × m^{-1} at the same temperature [39]. Some kind of compromise between values of electrical conductivity and Seebeck coefficient is achieved for charge carriers' concentration of 10^{19} cm^{-3}. For instance, type-VIII clathrate $Ba_8Ga_{16}Sn_{30}$ doped with small amounts of Cu demonstrates $S = 350$ μV × K^{-1} coexisting with $\sigma = 3 \times 10^4$ S × m^{-1} at 300 K [40].

Important value describing the entire charge carriers' transport is so-called power factor, *PF*, which is related to other properties as $PF = S^2 \sigma$ [2, 3]. Therefore, for more effective transport of charge carriers, both electrical conductivity and Seebeck coefficient should be maximized, which is impossible for intrinsic semiconductors. Consequently, attempts have been made to optimize charge carriers' concentration by multiple doping and/or vacancy formation. This may lead to altering the band structure by introducing donor and/or acceptor levels, which may be broad enough to cause their overlap with both conduction and valence bands, giving rise to properties of "bad metal" and, provided the optimal tuning is achieved, to metal-to-semiconductor transition. As a result of this strategy, combination of $S = 170\ \mu V \times K^{-1}$ with $\sigma = 4.75 \times 10^4\ S \times m^{-1}$ at 300 K was achieved for $Si_{46-x}P_xTe_{8-y}$, leading to $PF = 0.14 \times 10^{-3}\ W \times m^{-1} \times K^{-2}$, which is almost four orders of magnitude greater than that for ideally stoichiometric compound $Si_{30}P_{16}Te_8$ [30, 32].

As temperature increases, both electrical conductivity and Seebeck coefficient tend to grow (**Figure 7**), and therefore, power factor also increases; for instance, *PF* for $Ge_{31}P_{15}Se_8$ is three orders of magnitude higher at 650 K compared to 300 K [29].

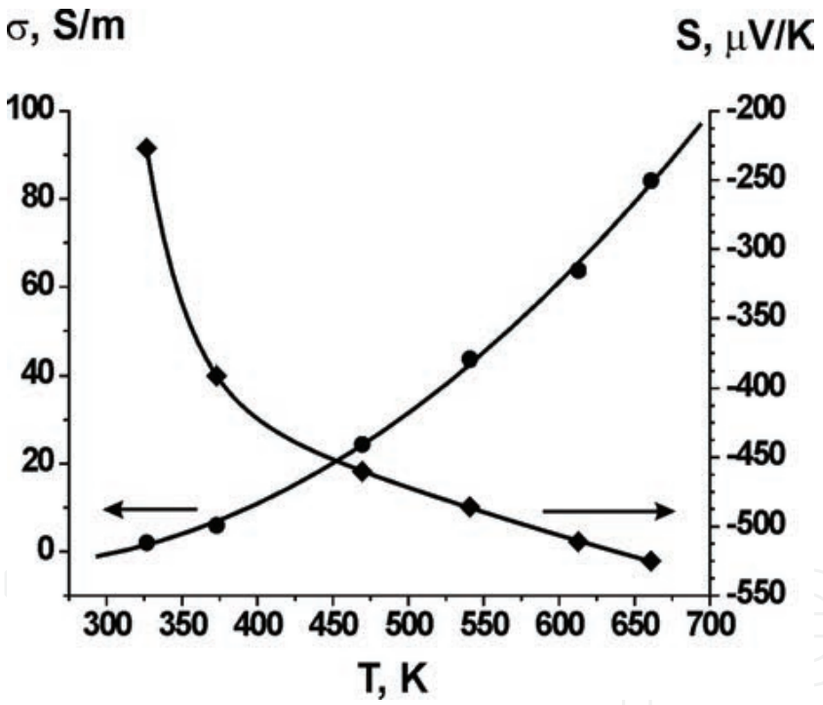

Figure 7. Electrical conductivity σ and Seebeck coefficient S of clathrate $Ge_{31}P_{15}Se_8$ as function of temperature.

4.2. Guest dynamics and heat transport

Clathrates are famous for their low, glass-like thermal conductivity, which originates from the details of their crystal structure, namely from the motion of guest atoms inside oversized cages of the framework (see **Figure 3b**). Such a motion is known as rattling; it provides pseudo-localized vibrations that are alien to concerted (Debye) vibrations of atoms composing the framework.

Analysis of atomic displacement parameters (ADPs) shows that in all types of clathrate compounds guest atoms have the highest values of ADPs and that absolute values depend on the nature of guest atom and degree of host-guest mismatch. As a rule, temperature dependence of ADPs is linear, which provides an opportunity to estimate characteristic Debye and Einstein temperatures, θ_D and θ_E, that are proportional to the slope of $<U^2>(T)$ function, where $<U^2>$ is the mean square atomic displacement either taken for any particular guest atom or averaged over all framework atoms. These characteristic temperatures describe dynamics of clathrate compounds. In particular, θ_D characterizes the framework; the higher the Debye temperature, the more rigid the framework. Value of θ_D depends primarily on the nature of atoms composing the framework. Si-based clathrates are known to be the most rigid, and their θ_D values may exceed 500 K [20]. Frameworks based on tin or germanium are less rigid, and θ_D value falls in the range of 150–320 K largely depending on the nature and concentration of doping element.

Einstein characteristic temperature provides information on pseudo-localized vibrations of guest atoms inside the framework. In general, its characteristics depend on type of clathrate crystals structure, on atomic mass and size of guest atom, and on host-guest mismatch for given clathrate compound.

Further analysis shows that in all clathrates, ADPs for guest atoms are always greater than for the framework ones. For instance, **Figure 8** displays temperature dependence of ADPs for crystal structure of cationic clathrate, in which framework is composed of silicon and phosphorus atoms in approximate ratio 2:1, whereas tellurium and selenium atoms jointly occupy guest positions.

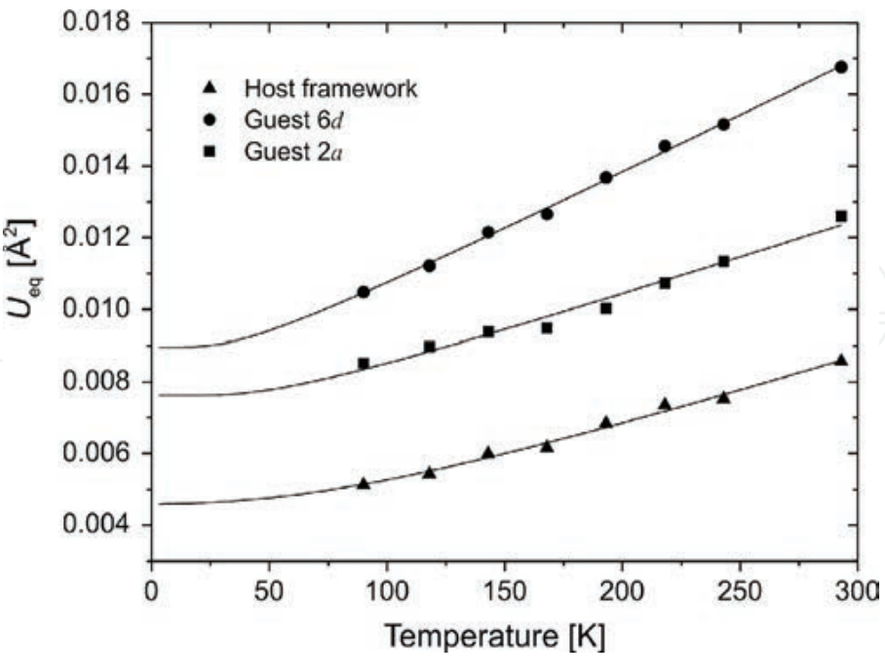

Figure 8. Temperature dependence of ADPs in crystal structure of type-I clathrate $[Si,P]_{46}Te_{6.78}Se_{1.22}$. Reprinted with permission from Inorg. Chem. 2012, 51, 11396–11405. Copyright 2012 American Chemical Society.

Clearly, ADPs averaged over the framework atoms are the lowest in the structure, ADP for guests in *2a* position comes next, and that for guest in 6*d* position is the highest. The difference between two guest positions is related to structural features. Effective volume of 20-vertex cage centered by 2*a* site is lower than that of 24-vertex cage centered at 6*d*. Moreover, 20-vertex cage is perfectly isotropic, whereas in 24-vertex cage (*cf*. **Figure 2**), motion in the direction of two hexagonal faces and that in perpendicular direction should occur at different frequencies. Such an anisotropy was clearly demonstrated for type-I clathrate $Sn_{24}P_{19.3}I_8$ [41]. **Figure 9** shows that, firstly, ADP of I2 atom residing in the center of 24-vertex cage is the largest in the system. Secondly, whereas motion of I1 atoms is described by single Einstein temperature of 76 K, displacement of I2 is characterized by two Einstein modes because of anisotropy of vibrations. In particular, axial movement in direction to hexagonal faces of tetrakaidecahedron occurs at lower frequency than that in perpendicular direction; respective values of θ_E are 79 and 63 K.

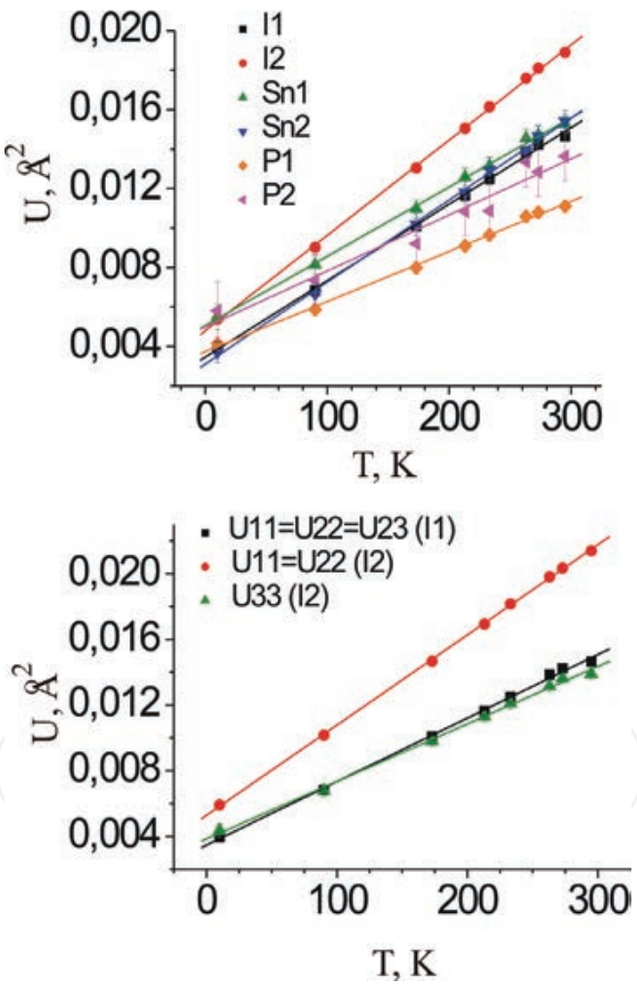

Figure 9. Temperature dependence of ADPs for $Sn_{24}P_{19.3}I_8$. (top) Equivalent ADPs for all atoms. (bottom) Guest atom ADPs in an anisotropic mode. Reprinted with permission from J. Alloys Compd. 2012, 520, 174–179. Copyright 2012 Elsevier.

Guest dynamics can be probed by various methods, ADPs analysis being just a most typical example. Other methods include direct or indirect observation of guest vibration frequencies

http://dx.doi.org/10.5772/65600

by means of Raman spectroscopy, inelastic neutron scattering, resonance ultrasound spectroscopy, heat capacity data, and other tools. Of them, low temperature examination of heat capacity data is frequently used to analyze jointly Debye and Einstein modes. Such analysis was performed for quite a number of clathrates. It was shown that no anomaly is observed below room temperature pointing at the absence of phase transitions, which is corroborated by linearity of $U(T)$ dependencies. At low temperatures, heat capacity of clathrates does not obey Debye law of cubes owing to significant contributions of Einstein modes. For type-I clathrate $Sn_{24}P_{19.3}I_8$ [41] described above, low-T part of $C_P(T)$ dependence could be circumscribed only by taking into account three different contributions, one Debye and two Einstein, that account for concerted vibrations of the entire framework and for two localized modes (**Figure 10**). Extracted values of θ_D (265 K) and θ_E (60 and 78 K) match to values obtained from ADPs [42].

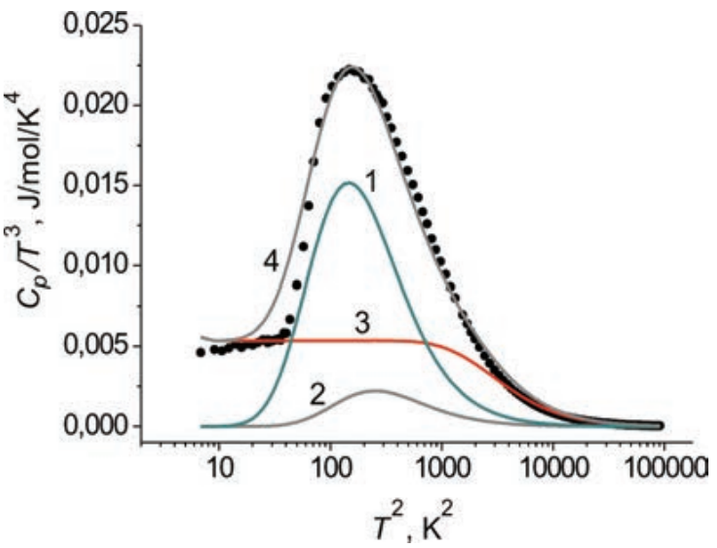

Figure 10. Plot of C_P/T^3 versus T^2 in semi-logarithmic coordinates. Two Einstein (1, 2) and one Debye (3) contributions to total C_p/T^3 values (4) are given in comparison with experimental data (filled circles). Reprinted with permission from J. Alloys Compd. 2012, 520, 174–179. Copyright 2012 Elsevier.

Lattice dynamics defines the principal contribution to thermal conductivity of clathrates. Although the majority of clathrates are low-gap semiconductors, they display very low values of thermal conductivity, which ranges at room temperature from 0.4 to 2.0 W × m^{-1} × K^{-1}. Rattling of guest atoms is the primary reason of reducing thermal conductivity of clathrates due to either lowering of phonon group velocity because of avoided crossing of acoustic modes or resonant scattering of phonons by rattling modes. However, other features of particular clathrate compounds can be added to the mechanism of reducing thermal conductivity. First, vacancy formation within the clathrate framework makes it less rigid leading to reducing Debye temperature, which, in turn, is proportional to velocity of sound, v_s, that is related to thermal conductivity as $\kappa_L = 1/3(v_s C_P \lambda)$, where κ_L is lattice part of thermal conductivity, C_P is heat capacity, and λ is phonon mean free path. Second, formation of superstructures gives rise to high unit volumes causing less concerted vibrations of framework atoms, thus reducing

thermal conductivity. Third, mass alternation within guest substructure alters phonon mean free path without affecting individual rattling modes, thus also reducing thermal conductivity. Finally, in real systems, any combination of these scenarios is possible.

Mass alternation leads to low thermal conductivity of mixed-guest clathrates $Sn_{24}P_{19.3}I_{8-x}Br_x$ (x = 2–4) [26]. For any composition *x*, thermal conductivity is lower than for single-guest compounds, although the latter phases already exhibit low thermal conductivity due to both guest rattling and vacancies within the framework. The lowest value of 0.5 W × m^{-1} × K^{-1} is observed at 300 K for composition with I:Br ratio of 1:1 (**Figure 11**), proving that mass alternation is the driving force for reducing thermal conductivity. Mass alternation brings about another peculiar effect as thermal conductivity of such clathrates is glass-like. Whereas for typical crystalline semiconductors thermal conductivity increases until temperature of about 30–50 K and then decreases as $\kappa = f(T^{-1})$, glass-like clathrates show smooth increase in thermal conductivity and then temperature-independent regime in the range of about 50–300 K (**Figure 11**).

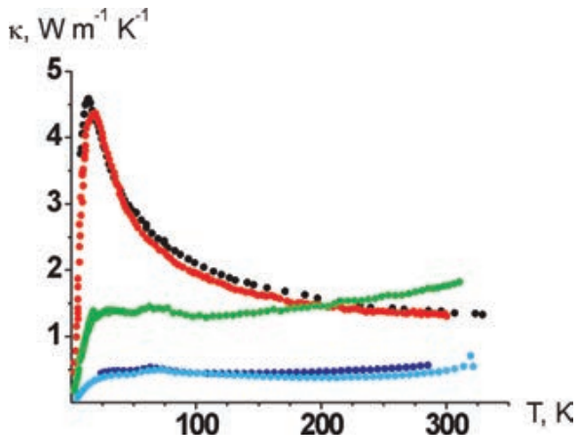

Figure 11. Temperature dependence of thermal conductivity for several clathrates: black, Cs_8Sn_{44}; red, $Ba_8Ga_{16}Ge_{30}$; green, $Sn_{24}P_{19.3}I_8$; blue, $Sn_{24}P_{19.3}I_4Br_4$; cyan, $Sn_{20.5}As_{22}I_8$.

Recently, it was shown that off-center displacement of guest atoms adds significantly to glass-like character of thermal conductivity; in particular, thermal conductivity of $Sr_8Ga_{16}Ge_{30}$ turns from crystalline-like to glass-like upon increasing off-center displacement of guest atoms sitting on 6*d* site [43].

Clathrate $Sn_{20.5}As_{22}I_8$ displays combination of eightfold cubic superstructure of type-I clathrates with vacancies and mixed occupancies of sites within the framework [31]. In response to structural features, this compound exhibits very low thermal conductivity with room-temperature value slightly over 0.4 W × m^{-1} × K^{-1}. Increasing complexity of the crystal structure by partial substitution of indium for tin results in further diminishing of thermal conductivity down to 0.36 W × m^{-1} × K^{-1} [16] (**Figure 11**).

$Ba_8Au_{16}P_{30}$ provides an example of peculiar orthorhombic superstructure of type-I structure with fivefold increase in the unit volume. In the region of 40–400 K, this compound demonstrates low, almost temperature-independent, thermal conductivity of 0.6 W × m^{-1} × K^{-1} [44]. However, this compound is not Zintl phase. It demonstrates metallic-like electrical conduc-

tance with resistivity slightly increasing with increased temperature. Therefore, another mechanism of thermal conductivity has substantial contribution to total thermal conductivity, which is electronic thermal conductivity. The latter is proportional to electrical conductivity, σ, according to Wiedemann-Franz equation $\kappa_e = L_0\sigma T$, where $L_0 = 2.45 \times 10^{-8}$ W × Ohm × K^{-2} is ideal temperature-independent Lorentz number and T is absolute temperature. It was shown that electronic part of thermal conductivity in $Ba_8Au_{16}P_{30}$ increases from 0.2 W × m^{-1} × K^{-1} at 100 K to slightly over 0.5 W × m^{-1} × K^{-1} at 400 K, meaning that at the same time lattice part of thermal conductivity decreases in the same interval from about 0.4 to even below 0.2 W × m^{-1} × K^{-1} at 400 K, which is the lowest documented value of lattice thermal conductivity for clathrates.

In rare cases, electronic part of thermal conductivity may play dominating role provided clathrate shows properties of good metallic conductor. Type-II clathrate $Na_{24}Si_{136}$ is example, showing dominating contribution of electronic thermal conductivity amounting at 24 W × m^{-1} × K^{-1} at room temperature [20].

4.3. Thermoelectric figure-of-merit

Analysis of transport properties of clathrates leads to conclusion that they possess high electrical conductivity up to 6.5×10^4 S/m, high absolute values of Seebeck coefficient up to ±800 μV/K, and low thermal conductivity down to 0.4 W × m^{-1} × K^{-1}. Were these values pertinent to single compound, its thermoelectric figure-of-merit would reach unbelievable values largely exceeding $ZT = 1$ at room temperature, which is benchmark of current state-of-the-art thermoelectric materials. However, due to the significant unavoidable coupling of charge carriers and heat transport, ZT values for clathrate compounds are quite low at room temperature, scarcely surpassing $ZT = 0.1$. Interestingly, the highest room-temperature ZT values are achieved for type-VIII clathrates. For instance, Sb-doped *p*-type $Ba_8Ga_{16}Sn_{30}$ demonstrates $ZT = 0.6$ and 300 K, whereas *n*-type $Ba_8Ga_{16}Sn_{30}$ displays $ZT = 0.5$ at the same temperature [45].

At higher temperature, as both electrical conductivity and Seebeck coefficient tend to grow, whereas thermal conductivity remains essentially constant (combination that is true for the majority of semiconducting clathrates), ZT increases with increasing temperature.

Type-I and type-II clathrates are the most studied species. Their thermoelectric properties have been reported in numerous papers, and, in general, it was shown that type-II clathrates rarely show promising thermoelectric properties due to the metallic properties that evoke low Seebeck coefficients of these compounds [6]. On the contrary, type-I clathrates demonstrate higher ZT with increasing temperature, with $Ba_8Ga_{16}Ge_{30}$ being the record holder displaying $ZT = 1.35$ at 900 K for Czochralski-pulled crystals [46].

Up to date, type-VIII clathrates demonstrate the highest values of ZT at elevated temperatures. These compounds are far less numerous than type-I and type-II counterparts, but, nevertheless, provide good examples of well-studied thermoelectric materials. In mid-temperature region, properly doped $Ba_8Ga_{16}Sn_{30}$ holds the record of the highest ZT. For n-type crystals grown from Ga flux and *p*-type crystals grown from Sn-flux display the highest thermoelectric efficiency. When properly doped, these compounds exhibit appreciable high values of ZT

reaching 1.45 at 500 K for Cu-doped *n*-type material and 1.0 at 480 K for Sb-doped *n*-type material [40, 47]. In general, prominent figures-of-merit can be reached only in the case of doped materials, even if doping is homovalent, but affords appropriate change in electronegativity and host-guest mismatch due to the adjustment of atomic radii. For instance, type-VIII clathrate $Sr_8Ga_{18}Ge_{30}$ does not display intriguing thermoelectric properties; however, partial substitution of Al for Ga affords $ZT = 0.56$ at 800 K [48]. Interestingly, replacement of guest Sr atoms by Eu ones leads to much poorer thermoelectric efficiency despite clearly similar atomic radii of these M^{2+} cations. The reason of this effect is not clear; probably, it is associated with magnetic structure of Eu-based analog. Moreover, this compound was reported to undergo second-order phase transition upon cooling to below 13 K followed by antiferromagnetic ordering that triggers giant magnetocaloric effect with magnetic entropy of 11.3 $J \times kg^{-1} \times K^{-1}$ [49]. Another example of increasing *ZT* upon introduction of magnetic cation is provided by $Ba_{6.9}Ce_{1.1}Au_6Si_{40}$, for which realization of Kondo interactions is believed to enhance the figure-of-merit by factor of 2 [11].

Because type-VIII clathrates demonstrate relatively poor thermal stability, their possible applications are limited by about 800 K, and they cannot be regarded as candidates for high-temperature thermoelectric power generation. Instead, silicon-based type-I and type-III clathrates are being investigated at high temperatures because of their utmost stability against oxidation in air [35]. In particular, cationic clathrates $Si_{31.9}P_{7.1}Te_{7.0}$ (type-I) and $Si_{132}P_{40}Te_{21.5}$ (type-III) are chemically and thermally stable up to 1200 K owing to several nanometers thin layers of phosphorus-doped silicon dioxide, which protects bulk samples from penetrating oxygen, that would lead to oxidation. Reported values of *ZT* for these Si-based clathrates do not exceed 0.4 (**Figure 12**); however, no attempts to increase the figure-of-merit have been performed so far.

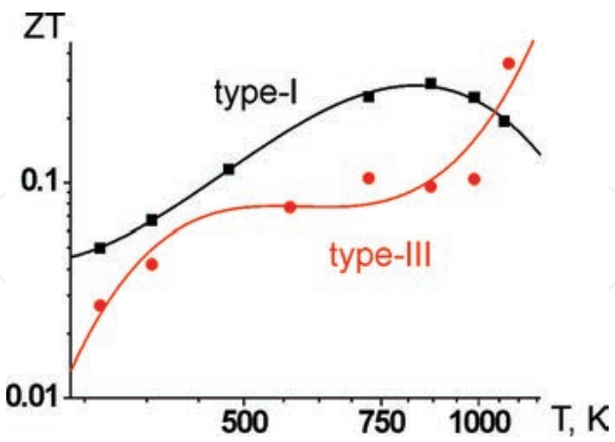

Figure 12. Figure-of-merit as function of temperature in double-logarithmic coordinates for type-I and type-III clathrates in Si-P-Te system.

Summarizing this section, it is worth noting that thermoelectric figure-of-merit for several clathrates of different structure types reaches 1.4–1.45 in the region of 500–800 K. The main tool for achieving such high values lies in the subtle doping of various low-gap clathrates that

http://dx.doi.org/10.5772/65600

causes simultaneous increase in electrical conductivity and Seebeck coefficient caused by proper doping accompanied by minor decrease in thermal conductivity caused by slight mass alteration.

5. Conclusion and outlook

Clathrates have been an attractive family of compounds primarily because of their fascinating structures. Within decades, it has become clear that clathrates are unique compounds combining spatial separation of host and guest substructures with very narrow (if any) band gaps, which allows almost independent optimization of charge carriers and thermal transport by tuning charge carriers' concentration and host-guest mismatch. Many chemical elements are known to take part in building clathrates frameworks of several types and serving as guests, making the property tuning plentiful and multifarious. With many instruments in hand, this tuning has already led to discovery of many clathrate compounds with carefully and wisely altered properties. Thermoelectric property optimization has been the central topic of clathrate research and resulted in various intriguing and promising achievements. They include, importantly, thermoelectric figure-of-merit almost reaching ZT = 1.5 in mid-T range and discovery of clathrates that demonstrate utmost stability in moist air at higher temperatures.

Nowadays, clathrates, albeit showing promising thermoelectric performance, are still far from commercial production and applications. Waiting for their explorations are elaboration of fabrication methods leading to *n*- and *p*-type legs of thermoelectric device, investigation of their compatibility at working temperature (from 500 to 1100 K), and engineering of contact and isolation layers. However, emerging sphere of automotive thermoelectric power generation requires new and more efficient thermoelectric materials capable of working at mid-T range being environmentally benign, whereas new trends in solar energy harvesting call for new thermoelectric materials exhibiting combination of high efficiency with outstanding chemical and thermal stability.

Nevertheless, clathrate research is an ongoing exploration. More than 300 papers are being published per annum in this decade on the topics ranging from the property optimization to uncovering of the underlying physics to elaboration of synthetic pathways and to discovery of new clathrates and related materials. Whereas the former topic works for near-future applications, the latter one is still of basic research. However, it shows that many new clathrates, including those of rare or even new types, are awaiting their discovery and property investigation.

Acknowledgements

This work is supported in part by the Russian Science Foundation under Grant # 16-12-00004.

Author details

Andrei V. Shevelkov

Address all correspondence to: shev@inorg.chem.msu.ru

Department of Chemistry, Lomonosov Moscow State University, Moscow, Russia

References

[1] Ioffe AF. Semiconductor Thermoelements and Thermoelectric Cooling. London: Infosearch Ltd.; 1957.

[2] Nolas GS, Cohn JL, Slack GA, Schjuman SB. Semiconducting Ge clathrates: promising candidates for thermoelectric applications. Appl. Phys. Lett. 1998; 73:178–180.

[3] Snyder GJ, Toberer ES. Complex thermoelectric materials. Nat. Mater. 2008; 7:105–114.

[4] Christensen M, Lock N, Overgaard J, Iversen BB. Crystal structures of thermoelectric n- and p-type $Ba_8Ga_{16}Ge_{30}$ studied by single crystal, multitemperature, neutron diffraction, conventional X-ray diffraction and resonant synchrotron X-ray diffraction. J. Amer. Chem. Soc. 2006; 128:15657–15665.

[5] Shevelkov AV, Kovnir KA, Zaikina JV. Chemistry and Physics of Inverse (Cationic) Clathrates and Tin Anionic Clathrates. In: The Physics and Chemistry of Inorganic Clathrates. Nolas GS, editor. Dorchester: Springer; 2014. pp. 125–167.

[6] Beekman M, Nolas GS. Inorganic clathrate-II materials of group 14: synthetic routes and physical properties. J. Mater. Chem. 2008; 18:842–851.

[7] Slack GA. New Materials and Performance Limits for Thermoelectric Cooling In: CRC Handbook of Thermoelectrics. Rowe DM, editor. Boca Raton, FL: CRC Press; 1995.

[8] Kasper JS, Hagenmuller P, Pouchard M, Cros C. Clathrate structure of silicon Na_8Si_{46} and Na_xSi_{136} ($x < 11$). Science. 1965; 150:1713–1714.

[9] Kirsanova MA, Olenev AV, Abakumov AM, Bykov MA, Shevelkov AV. Extension of the clathrate family: type-X clatrhate $Ge_{79}P_{29}S_{18}Te_6$. Angew. Chem. Int. Ed. 2011; 50:2371–2374.

[10] Kirsanova MA, Shevelkov AV. Clathrates and semiclathrates of Type-I: crystal structure and superstructures. Z. Kristallogr. 2013; 228:215–227.

[11] Prokofiev A, Sidorenko A, Hradil K, Ikeda M, Svagera R, Waas M, Winkler H, Neumaier K, Paschen S. Thermopower enhancement by encapsulating cerium in clathrate cages. Nat. Mater. 2013; 12:1096–1101.

[12] Kovnir K, Stockert U, Budnyk S, Prots Y, Baitinger M, Paschen S, Shevelkov AV, Grin Y. Introducing a magnetic guest to a tetrel-free clathrate: synthesis, structure, and properties of $Eu_xBa_{8-x}Cu_{16}P_{30}$ ($0 \le x \le 1.5$). Inorg. Chem. 2011; 50:10387–10396.

[13] Bentien A, Pacheco V, Paschen S, Grin Y, Steglich F. Transport properties of composition tuned α- and β–$Eu_8Ga_{16-x}Ge_{30+x}$. Phys. Rev. B. 2005; 71:165206.

[14] Shevelkov AV, Kovnir K. Zintl Clathrates. In: Structure and Bonding, Vol. 139 (Zintl Phases). Fässler TF, editor. Berlin, Heidelberg: Springer-Verlag; 2011. pp. 97–142.

[15] Mingos DM. Essential Trends in Inorganic Chemistry. Oxford: Oxford University Press; 1998.

[16] Kelm EA, Olenev AV, Bykov MA, Sobolev AV, Presniakov IA, Kulbachinskii VA, Kytin VG, Shevelkov AV. Synthesis, crystal structure, and thermoelectric properties of clathrates in the Sn-In-As-I system. Z. Anorg. Allg. Chem. 2011; 637:2059–2067.

[17] Shatruk MM, Kovnir KA, Shevelkov AV, Presniakov IA, Popovkin BA. First tin pnictidehalides $Sn_{24}P_{19.3}I_8$ and $Sn_{24}As_{19.3}I_8$: synthesis and the clathrate-I type of the crystal structure. Inorg. Chem. 1999; 38:3455–3457.

[18] Yashina LV, Volykhov AA, Neudachina VS, Aleksandrova NV, Reshetova LN, Tamm ME, Pérez-Dieste V, Escudero C, Vyalikh DV, Shevelkov AV. Experimental and computational insight into the chemical bonding and electronic structure of clathrate compounds in the Sn–In–As–I system. Inorg. Chem. 2015; 54:11542–11549.

[19] Beekman M, Sebastian CP, Grin Yu, Nolas GS. Synthesis, crystal structure, and transport properties of $Na_{22}Si_{136}$. J. Electron. Mater. 2009; 38:1136–1141.

[20] Beekman M, Schnelle W, Borrmann H, Baitinger M, Grin Y, Nolas GS. Intrinsic electrical and thermal properties from single crystals of $Na_{24}Si_{136}$. Phys. Rev. Lett. 2010; 104:018301.

[21] Zaikina JV, Kovnir KA, Haarmann F, Schnelle W, Burkhardt U, Borrmann H, Schwarz U, Grin Y, Shevelkov AV. The first silicon-based cationic clathrate III with high thermal stability: $Si_{172-x}P_xTe_y$ (x=2y, y>20). Chem. Eur. J. 2008; 14:5414–5422.

[22] Kovnir KA, Sobolev AV, Presniakov IA, Lebedev OI, Van Tendeloo G, Schnelle W, Grin Y, Shevelkov AV. $Sn_{19.3}Cu_{4.7}As_{22}I_8$: a new clathrate-I compound with transition-metal atoms in the cationic framework. Inorg. Chem. 2005; 44:8786–8793.

[23] Kovnir KA, Shatruk MM, Reshetova LN, Presniakov IA, Dikarev EV, Baitinger M, Haarmann F, Schnelle W, Baenitz M, Grin Y, Shevelkov AV. Novel compounds $Sn_{20}Zn_4P_{22-v}I_8$ (v=1.2), $Sn_{17}Zn_7P_{22}I_8$, and $Sn_{17}Zn_7P_{22}Br_8$: synthesis, properties, and special features of their clathrate-like crystal structures. Solid State Sci. 2005; 7:957–968.

[24] Condron CL, Martin J, Nolas GS, Piccoli PMB, Schultz AJ, Kauzlarich SM. Structure and thermoelectric characterization of $Ba_8Al_{14}Si_{31}$. Inorg. Chem. 2006; 45:9381–9386.

[25] Avila MA, Suekuni K, Umeo K, Fukuoka H, Yamanaka S, Takabatake T. Glasslike versus crystalline thermal conductivity in carrier-tuned $Ba_8Ga_{16}X_{30}$ clathrates (*X*=Ge,Sn). Phys. Rev. B. 2006; 74:125109.

[26] Zaikina JV, Schnelle W, Kovnir KA, Olenev AV, Grin Y, Shevelkov AV. Crystal structure, thermoelectric and magnetic properties of the type-I clathrate solid solutions $Sn_{24}P_{19.3(2)}Br_xI_{8-x}$ ($0 \le x \le 8$) and $Sn_{24}P_{19.3(2)}Cl_yI_{8-y}$ ($y \le 0.8$). Solid State Sci. 2007; 9:664–671.

[27] Dumont-Botto E, Bourbon C, Patoux S, Rozier P, Dolle M. Synthesis by spark plasma sintering: a new way to obtain electrode materials for lithium ion batteries. J. Power Sources. 2011; 196:2274–2278.

[28] Jaussaud N, Toulemonde P, Pouchard M, San Miguel A, Gravereau P, Pechev S, Goglio G, Cros C. High pressure synthesis and crystal structure of two forms of a new tellurium-silicon clathrate related to the classical type I. Solid State Sci. 2004; 6:401–404.

[29] Kirsanova MA, Mori T, Maruyama S, Matveeva M, Batuk D, Abakumov AM, Gerasimenko AV, Olenev AV, Grin Y, Shevelkov AV. Synthesis, structure, and transport properties of type-I derived clathrate $Ge_{46-x}P_xSe_{8-y}$ (x = 15.4(1); y = 0–2.65) with diverse host-guest bonding. Inorg. Chem. 2013; 52:577–588.

[30] Zaikina JV, Kovnir KA, Burkhardt U, Schnelle W, Haarmann F, Schwarz U, Grin Y, Shevelkov AV. Cationic clathrate I $Si_{46-x}P_xTe_y$ ($6.6(1) \le y \le 7.5(1)$, $x \le 2y$): crystal structure, homogeneity range, and physical properties. Inorg. Chem. 2009; 48:3720–3730.

[31] Zaikina JV, Kovnir KA, Sobolev AV, Presniakov IA, Prots Y, Baitinger M, Schnelle W, Olenev AV, Lebedev OI, Van Tendeloo G, Grin Y, Shevelkov AV. $Sn_{20.53.5}As_{22}I_8$: a largely disordered cationic clathrate with a new type of superstructure and abnormally low thermal conductivity. Chem. Eur. J. 2007; 13:5090–5099.

[32] Kishimoto K, Koyanagi T, Akai K, Matsuura M. Synthesis and thermoelectric properties of type-I clathrate compounds $Si_{46-x}P_xTe_8$. Jap. J. Appl. Phys. 2007; 46:L746–L748.

[33] Hayashi M, Kishimoto K, Akai K, Asada H, Kishio KT, Koyanagi K. Preparation and thermoelectric properties of sintered n-type $K_8M_8Sn_{38}$ (M = Al, Ga and In) with the type-I clathrate structure. J. Phys. D Appl. Phys. 2012; 45:455308.

[34] Yakimchuk AV, Zaikina JV, Reshetova LN, Ryabova LI, Khokhlov DR, Shevelkov AV. Impedance of $Sn_{24}P_{19.3}Br_xI_{8-x}$ semiconducting clathrates. Low Temp. Phys. 2007; 33:276–279.

[35] Zaikina JV, Mori T, Kovnir K, Teschner D, Senyshyn A, Schwarz U, Grin Y, Shevelkov AV. Bulk and surface structure and high-temperature thermoelectric properties of inverse clathrate-III in the Si-P-Te system. Chem. Eur. J. 2010; 16:12582–12589.

[36] Fukuoka H, Kiyoto J, Yamanaka S. Superconductivity of metal deficient silicon clathrate compounds, Ba8-*x*Si46 ($0 < x < 1.4$). Inorg. Chem. 2004; 42:2933–2937.

[37] Yuan HQ, Grosche FM, Carrillo-Cabrera W, Paschen S, Sparn G, Baenitz M, Grin Y, Steglich F. High-pressure studies on a new superconducting clathrate: Ba_6Ge_{25}. J. Phys. Condens. Matter. 2002; 14:11249.

[38] Bobev S, Sevov SC. Synthesis and characterization of stable stoichiometric clathrates of silicon and germanium: $Cs_8Na_{16}Si_{136}$ and $Cs_8Na_{16}Ge_{136}$. J. Amer. Chem. Soc. 1999; 121:3795–3796.

[39] Kishimoto K, Arimura S, Koyanagi T. Preparation and thermoelectric properties of sintered iodine-containing clathrate compounds $Ge_{38}Sb_8I_8$ and $Sn_{38}Sb_8I_8$. Appl. Phys. Lett. 2006; 88:222115.

[40] Saiga Y, Dua B, Deng SK, Kajisa K, Takabatake T. Thermoelectric properties of type-VIII clathrate $Ba_8Ga_{16}Sn_{30}$ doped with Cu. J. Alloys Compd. 2012; 537:303–307.

[41] Novikov VV, Matovnikov AV, Avdashchenko DV, Mitroshenkov NV, Dikarev EV, Takamizawa S, Kirsanova MA, Shevelkov AV. Low-temperature structure and lattice dynamics of the thermoelectric clathrate $Sn_{24}P_{19.3}I_8$. J. Alloys Compd. 2012; 520:174–179.

[42] Kovnir KA, Zaikina JV, Reshetova LN, Olenev AV, Dikarev EV, Shevelkov AV. Unusually high chemical compressibility of normally rigid type-I clathrate framework: synthesis and structural study of $Sn_{24}P_{19.3}Br_xI_{8-x}$ solid solution, the prospective thermoelectric material. Inorg. Chem. 2004; 43:3230–3236.

[43] Christensen S, Schmøkel MS, Borup KA, Madsen GKH, McIntyre GJ, Capelli SC, Christensen M, Iversen BB. "Glass-like" thermal conductivity gradually induced in thermoelectric Sr8Ga16Ge30 clathrate by off-centered guest atoms. J. Appl. Phys. 2016; 119:185102.

[44] Fulmer J, Lebedev OI, Roddatis VV, Kaseman DC, Sen S, Dolyniuk JA, Lee K, Olenev AV, Kovnir K. Clathrate $Ba_8Au_{16}P_{30}$: the "Gold Standard" for lattice thermal conductivity. J. Am. Chem. Soc. 2013; 135:12313–12323.

[45] Saiga Y, Suekuni K, Deng SK, Yamamoto T, Kono Y, Ohya N, Takabatake T. Optimization of thermoelectric properties of type-VIII clathrate $Ba_8Ga_{16}Sn_{30}$ by carrier tuning. J. Alloys Compd. 2010; 507:1–5.

[46] Saramat A, Svensson G, Palmqvist AEC, Stiewe C, Mueller E, Platzek D, Williams SGK, Rowe DM, Bryan JD, Stucky GD. Large thermoelectric figure of merit at high temperature in Czochralski-grown clathrate Ba8Ga16Ge30J. Appl. Phys. 2006; 99:023708.

[47] Kono Y, Ohya N, Saiga Y, Suekuni K, Takabatake T, Akai K, Yamamoto S. Carrier doping in the type VIII clathrate $Ba_8Ga_{16}Sn_{30}$. J. Electr. Mat. 2011; 40:845–850.

[48] Sasaki Y, Kishimoto K, Koyanagi T, Asada H, Akai K. Synthesis and thermoelectric properties of type-VIII germanium clathrates $Sr_8Al_xGa_yGe_{46-x-y}$. J. Appl. Phys. 2009; 105:073702.

[49] Phan MH, Woods GT, Chaturvedi A, Stefanoski S, Nolas GS, Srikanth H. Long-range ferromagnetism and giant magnetocaloric effect in type VIII $Eu_8Ga_{16}Ge_{30}$ clathrates. Appl. Phys. Lett. 2008; 93:252505.

IntechOpen